Title
Characterization of the spectral phase of an intense laser at focus via ionization blueshift

Journal
Journal of the Optical Society of America B, 33(9)

ISSN
0740-3224

Authors
Mittelberger, DE
Nakamura, K
Lehe, R
et al.

Publication Date
2016-09-01

DOI
10.1364/josab.33.001978

Peer reviewed

Characterization of the Spectral Phase of an Intense Laser at Focus via Ionization Blueshift

D. E. Mittelberger[1,2], K. Nakamura[1], R. Lehe[1], A. J. Gonsalves[1], C. Benedetti[1], H.-S. Mao[1], J. Daniels[1,3], N. Dale[1,2], S. V. Venkatakrishnan[1], K. K. Swanson[1,2], E. Esarey[1], and W. P. Leemans[1,*]

[1] *Lawrence Berkeley National Laboratory, Berkeley CA 94720, USA*
[2] *University of California - Berkeley, Berkeley CA 94720, USA*
[3] *Eindhoven University of Technology, Eindhoven, The Netherlands*
[*] *Corresponding author: WPLeemans@lbl.gov*

Compiled July 25, 2016

An in-situ diagnostic for verifying the spectral phase of an intense laser pulse at focus is presented. This diagnostic relies on measuring the effect of optical compression on ionization-induced blueshifting of the laser spectrum. Experimental results from the Berkeley Lab Laser Accelerator (BELLA), a laser source rigorously characterized by conventional techniques, are presented and compared with simulations to illustrate the utility of this technique. These simulations show distinguishable effects from second, third, and fourth order spectral phase.

OCIS codes: *(050.5080) Phase shift; (070.4340) Nonlinear optical signal processing; (190.2640) Stimulated scattering, modulation, etc.; (190.7110) Ultrafast nonlinear optics*

http://dx.doi.org/10.1364/ao.XX.XXXXXX

1. INTRODUCTION

The frontiers of high intensity optical physics, such as laser plasma acceleration (LPA) [1] and high harmonic generation (HHG) [2], have expanded rapidly with the development of chirped pulse amplification (CPA) laser systems that can produce high-peak-power laser pulses [3]. The production of stable, high quality electron beams from LPA systems in particular requires precise knowledge and control of the driving laser. It has been shown that chirp and asymmetry in the temporal profile of the driving laser pulse can affect the energy and bunch charge of accelerated electrons even for laser pulses of the same peak power and pulse duration [4]. Although spectral bandwidth sets a lower limit on compressed pulse width, the phase of a laser's spectrum ultimately determines the temporal pulse profile and residual chirp for any particular pulse compression. Knowledge of spectral phase is thus crucial for characterizing a CPA system.

Various techniques have been developed to characterize pulse duration, intensity envelope shape, chirp, and spectral phase [5]. These methods generally rely on a signal created via one or more nonlinear crystals (e.g., second and third order autocorrelation, Frequency-Resolved Optical Gating [6]) which requires significant attenuation of the full laser energy. In addition, these techniques and direct measurements such as SPIDER [7] cannot measure spectral properties at focus except by imaging the vacuum focus through a window or other transmissive optics, which introduce additional dispersion. Knowledge of the focused pulse properties is of critical importance for controlling laser-plasma interactions. Previous works [8–10] have demonstrated the extrapolation of spectral phase information from the blueshifted spectrum of a pulse ($I \sim 10^{11}\,\mathrm{W/cm^2}$) propagated through a medium with nonlinear index of refraction. In this article, these results are extended to higher intensities ($I \sim 10^{16}\,\mathrm{W/cm^2}$) to allow in-situ evaluation of ionizing laser pulses at the target. Other works have demonstrated that at higher intensities ($I \sim 10^{18}\,\mathrm{W/cm^2}$) the laser's wake in the ionized plasma causes blueshifting and photon acceleration [11, 12].

We propose analyzing the spectral phase of an ionizing pulse from the morphology of its blueshifted spectrum as a function of pulse compression. Measuring the dependence of blueshifting on the compressed pulse's chirp and intensity adds additional constraints to the laser phase, which are necessary because of the highly nonlinear interaction of the ionizing pulse. Pulse characterization from the spectral morphology has several advantages over currently available techniques. The blueshifting effect probes the spectral phase in-situ near target and can characterize the laser pulse with only simple spectral measurements before and after the interaction. Specifically, this technique only requires a spectrometer and an optical compressor that can be scanned, which are components of typical chirped pulse amplification laser systems, as well as a way to characterize the target density. Although the initial phase cannot be calculated

analytically from the pattern of spectral morphology, the clear dependence of blueshifting morphology on spectral phase and the independent effects of different orders of phase, as is demonstrated below, show that phase determination is possible by iterative simulations.

We first analyze the spectral blueshifting of an intense laser pulse propagating through and ionizing a gas target and introduce a numerical simulation to make quantitative predictions of blueshifted spectra. The effects of chirp and optical compression on the blueshifted spectrum are explored. We then discuss the effects of focusing, pulse evolution, and target density profile. The application of these phenomena to characterize spectral properties of laser systems is discussed, and simulation results are compared with a series of measurements performed at the Berkeley Lab Laser Accelerator (BELLA) to set representative limits on the sensitivity of this technique to different orders of phase.

2. SPECTRAL BLUESHIFTING OF AN IONIZING PULSE

In a typical LPA scheme, a compressed pulse from a CPA laser is focused through a neutral gas target with a peak focal intensity much higher than the ionization threshold, I_{thresh}, of the target gas [1]. The output spectrum is a complex function of the input laser pulse's temporal structure (envelope & chirp), its focusing ($I_{peak}(z)$), and the density profile of the ionizing gas [13, 14]. To understand the laser interaction, the spatial distribution of neutral gas must be determined via a secondary diagnostic such as interferometry. As the intense laser pulse propagates through an LPA target, it ionizes the neutral gas. Hence, the front of the laser pulse travels through a lower plasma density than the rear of the pulse (Fig. 1), and the phase velocity increases (and the index of refraction η decreases) toward the rear. In general, a gradient in phase velocity in the co-moving frame of a laser pulse causes a shift in frequency proportional to the gradient. This results from phasefronts with different speeds moving closer together or further apart, depending on the sign of the gradient, as the pulse propagates. In an unmagnetized, underdense plasma, the phasefront speed is

$$v_{phase} = c/\eta = c\left(1 - \omega_p^2/\omega^2\right)^{-1/2} \quad (1)$$

where η is the index of refraction, ω is the laser's instantaneous frequency and $\omega_p \propto n_{plasma}^{1/2}$ is the plasma frequency. The gradient in the plasma density, n_{plasma}, inside an ionizing laser leads to a change in frequency

$$\frac{\partial \omega}{\partial z} = -\frac{\omega_p}{\omega}\frac{\partial \omega_p}{\partial \xi} \quad (2)$$

at position $\xi = z - ct$ in the pulse [1, 15]. The plasma density, and therefore plasma frequency, decreases toward the front of the pulse, causing the phasefronts to compress in the ionizing region and shifting the spectrum in that region toward shorter wavelengths (i.e. blueshifting). The spatial location of the blueshifted region in the pulse envelope is set by the position in the co-moving frame where the intensity of the pulse reaches the ionization threshold for the gas ($I_{thresh} \approx 2.8 \times 10^{14}\,\mathrm{W/cm^2}$ for H_2 [16]). The ionization threshold for the ADK (Ammosov-Delone-Krainov) tunneling ionization model [17] can be defined as the intensity where the ionization probability transitions from exponential to linear as a function of intensity. The location of the ionization front is recorded in the spectrum of a chirped pulse since the pulse's instantaneous frequency varies with position. Referring to Eqn. 2, the magnitude of the spectral shift is proportional to the gradient in plasma density, so a higher density target will give a larger spectral shift.

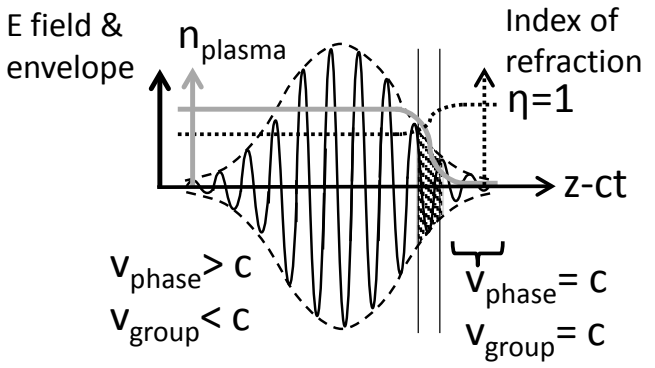

Fig. 1. Schematic of an ionizing pulse propagating through an initially unionized gas. The shading indicates the frequency blueshifted section of the pulse where most ionization occurs. Propagation is from left to right.

The spectral shift of a chirped pulse contains information about the instantaneous frequency at the ionization front, which is related to the complex spectrum. The electric field of a broadband laser pulse can be written as

$$\left|\widetilde{E}(\omega)\right| e^{i\phi(\omega)} = \mathcal{F}\left\{|E(t)|\, e^{i\omega_0 t + i\theta(t)}\right\} \quad (3)$$

where the time domain components are the spectrum's central frequency ω_0 and non-linear chirp $\theta(t)$. The frequency domain parameter is the total spectral phase $\phi(\omega)$, and the two are related by a Fourier transform $\mathcal{F}$. Typically, the spectral phase is described as a perturbation series around the central frequency

$$\phi(\omega) = \sum_{n=0}^{\infty} \frac{1}{n!}\frac{\partial^n \phi}{\partial \omega^n}(\omega - \omega_0)^n. \quad (4)$$

Knowledge of high-order spectral phase is of interest because it limits laser pulse compression and is the cause of temporal asymmetry and nonlinear chirp in the compressed pulse, which affect electron acceleration [1, 4]. Even in a CPA laser that is optimally compressed, the laser pulse typically has residual nonlinear chirp due to high-order dispersion in the amplifier and transport optics.

By varying the grating spacing in the ionizing pulse's optical compressor, the blueshifted spectra can probe the dependence of nonlinear chirp on pulse compression, which is related to the spectral phase by a Fourier transform. This variation of chirp with compression is recorded in the morphology of blueshifted spectra versus compressor grating spacing. If the gas distribution of the target is known, then measurements of the blueshifted spectrum can provide an in-situ diagnostic of the pulse's spectral phase near focus using a numerical simulation to understand the complex interaction. Along with a model of pulse compression, the blueshifted spectra thus act as a diagnostic of high-order spectral phase of the laser system (i.e. the phase of the uncompressed laser). This diagnostic can either be used to verify the spectral phase at focus from an independent measurement of complex spectrum, or test a hypothesized initial phase and then iteratively determine the true spectral phase.

3. NUMERICAL SIMULATION OF EXPERIMENTAL SETUP AND BLUESHIFTING

A version of the 2D-cylindrical laser-plasma interaction simulation code INF&RNO [18, 19] was modified to include ionization and neglect plasma motion. Plasma motion is typically negligible at these laser intensities and neglecting it speeds up the calculations significantly. INF&RNO includes nonlinear laser evolution (e.g., relativistic self-focusing, ionization defocusing) and was used to simulate the ionizing laser's propagation through the neutral gas target and resulting blueshifting. This simulation code has been validated by extensive comparison with experiments [20–24] and is widely used to model the laser-plasma interaction at BELLA.

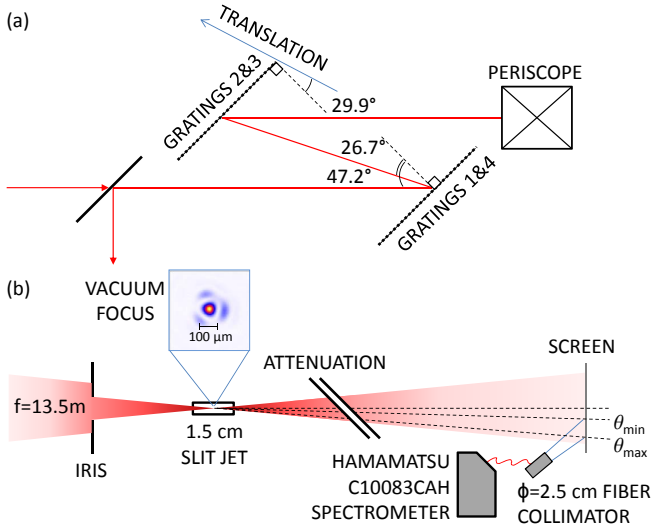

Fig. 2. Experimental setup modeled in these simulations showing (a) optical compressor with angles of incidence and diffraction on the first and final gratings and (b) target interaction and spectrometer light collection. The minimum and maximum angles of acceptance of the spectrometer are drawn. Note the schematic is not to scale.

The propagation of an intense laser through an ionizing target is simulated for a range of temporal profiles, resulting in a map of spectral blueshifting as a function of diffraction grating spacing. The morphology of the blueshifted spectra resulting from this series of simulations reveals the initial phase of the laser spectrum. For each simulated optical grating separation, the initial laser profile is calculated from either a Gaussian or a measured spectrum with a fixed spectral phase specified from measurements or test values. The additional phase contribution from the optical compressor is calculated from a high order model of compression [25, 26], and the complex spectrum is Fourier transformed into the time domain to yield the pulse's longitudinal profile and nonlinear chirp. For these simulations, the BELLA optical compressor was simulated, which consists of four matched 1480 line/mm gold-coated optical gratings as shown in Fig. 2a. The initial transverse profile is assumed to be either a Gaussian or a more-realistic Airy pattern, corresponding to a top hat near field profile, given by

$$E(r) = \begin{cases} E_0 e^{-(r/w_0)^2} \\ 2E_0 J_1(kr/w_0)/(kr/w_0) \end{cases} \quad (5)$$

where k=2.5838…The initial pulse is input at focus into INF&RNO, and the resulting propagated electric field is then transformed into the spectral domain. This can be done by calculating the full 3D electric field and taking a Fourier Transform with respect to each axis. In this work we recover the spectrum via the more efficient Hankel Transform with respect to r, which is much faster because it works with the electric field in the $r-z$ plane rather than the full 3D field. The fiber-coupled spectrometer used in these experiments collected an off-axis 2.5 cm diameter portion of the approximately 8.5 cm diameter beam (15.0 cm without iris) from a diffuse scattering screen (Fig. 2b). This needs to be taken into account because the blueshifting spectrum depends strongly on angle as a result of ionization defocusing. The integrated spectrum within the 2.5 cm circular aperture located 2.75 cm off axis was calculated as follows. First, the electric field is transformed into k-space by taking the Fourier Transform (implemented as a Fast Fourier Transform) of the electric field with respect to z and the Hankel transform with respect to r. The k-vectors which enter the angular acceptance window defined by the circular off-axis aperture (θ_{min} and θ_{max} in Fig. 2b) are then selected. For each frequency $\omega = ck_z$, a weighted sum is performed on the magnitude squared of the electric field, with a weighting function given by the azimuthal extent of an arc intersecting the aperture. This weighting function accounts for the varying light collected at different k-vector angles (Fig. 3). The transformation to frequency assumes $k_z \gg k_r$, which is accurate for a small detector located far from the target and close to the optical axis. This is illustrated in Fig. 3.

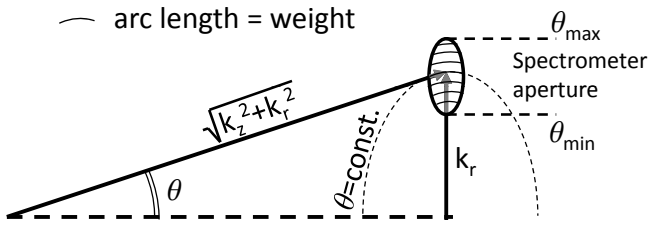

Fig. 3. A k-vector is shown which satisfies the angular limits set by the collection aperture: $\theta_{min} \leq \theta \leq \theta_{max}$. The magnitude squared of the electric field corresponding to this k-vector will be included in the spectral sum for frequency ω, weighted by length of the intersection of the $\theta =$ const. line and the circular aperture.

INF&RNO includes a self-consistent model of laser pulse propagation, but does not include the linear Kerr effect nor the high order Kerr effect (HOKE) on the front edge of the laser passing through neutral gas. These effects are not strong in the regime under consideration. The linear Kerr effect can be neglected because the beams being simulated have peak intensities in the interaction $I_{peak} \gg I_{thresh}$, and the effect is negligible in comparison with ionization defocusing. As an example of this, consider a transform-limited 80 mJ pulse focused to a 52 μm ($1/e^2$ intensity) Gaussian profile with a 31 fs pulse length (FWHM). This pulse will have a peak intensity of 5×10^{16} W/cm^{-3}, well above the ionization threshold for both hydrogen and helium. Based on the magnitude of the shift in index of refraction, ionization defocusing becomes more important than the linear Kerr effect when the intensity rises to only 5.5×10^{13} W/cm^{-2}, so just 4% of the pulse energy is more strongly affected by the Kerr effect. HOKE is not modeled be-

cause the effect is negligible for helium and other noble gasses [27].

The importance of ionization defocusing on the pulse propagation and final spectrum can not be overstated. Simulations show that ionization defocusing dominates diffraction in determining the evolution of pulse intensity, at least within a few Rayleigh lengths of focus. Further, the output spectrum has a strong angular dependance as a result of the ionization front's lensing effect, with more blueshifted light having a generally larger deflection. Initial 2D ray tracing simulations which included the phase shift in the laser fields from ionization, but not the effect on pulse propagation, yielded qualitatively different blueshifted spectra. For these reasons, any model of the interaction used for retrieving the spectral phase must include self-consistent laser propagation in the ionizing medium.

The goal of this simulation is to determine the unknown spectral phase from measured blueshifted spectra at various optical compression settings, but inverting the simulation (i.e. going from blueshifted spectra to initial pulse) is complicated by the highly nonlinear propagation of the ionizing pulse. We will demonstrate that it is possible to accurately model the resulting spectra for various initial spectral phases and determine limits to the technique's sensitivity to each order of phase. Development of an iterative method algorithm to test values of initial spectral phase and compare the resulting spectral morphology with measured results, however, is not addressed in this work.

The pattern of blueshifting is sensitive to initial second, third, and fourth order dispersion and each order of spectral phase affects the structure of blueshifted spectra differently. The blueshifted spectrum is sensitive in principle to higher orders of initial spectral phase as well. The different effects on the compressed pulses and corresponding on-axis (i.e. from the on-axis field rather than an off-axis near-field aperture, for simplicity) simulated blueshifted spectra are shown in Fig. 4. In these examples, an 80 mJ pulse is focused to a 52 μm Gaussian vacuum focal spot ($1/e^2$ radius) in the center of a 3 mm long jet of neutral hydrogen gas ($n_{H_2} = 1 \times 10^{18}\,\mathrm{cm}^{-3}$). These parameters, which differ from the experimental conditions below, were chosen to make the blueshifting morphology as clear as possible. The initial intensity profiles for different compressor grating spacings are shown on the left and the resulting on-axis blueshifted spectra after propagation through gas are shown on the right. Fig. 4a demonstrates the morphology from pulses which are transform limited at compression. Second order phase ϕ_2 sets the optical compressor position at which the pulse's chirp changes sign. In the temporal profile, this corresponds to the location where the pulse changes from red-first to blue-first, so in the spectral morphology, blueshifting of the spectrum and resulting spectral interference changes sides of the spectrum. For example, if the pulse is positively chirped the front of the pulse will be blueshifted to the same frequency as some location further back, and the temporal phase difference will result in interference in the spectral domain. This is demonstrated in Fig. 4a.

Initial third order phase ϕ_3 reduces the chirp of the main pulse and adds pre-/post-pulses to the intensity profile which contain much of the broadband spectral content of the pulse (Fig. 4b left plots). If negative third order phase is added, a region of the pre-pulses will blueshift and spectrally interfere with the remainder of the pulse, increasing the number of fringes in the spectral morphology. If positive phase is instead added, the now-less-chirped main pulse will be blueshifted and will interfere with only a small band of frequencies in the post-pulses,

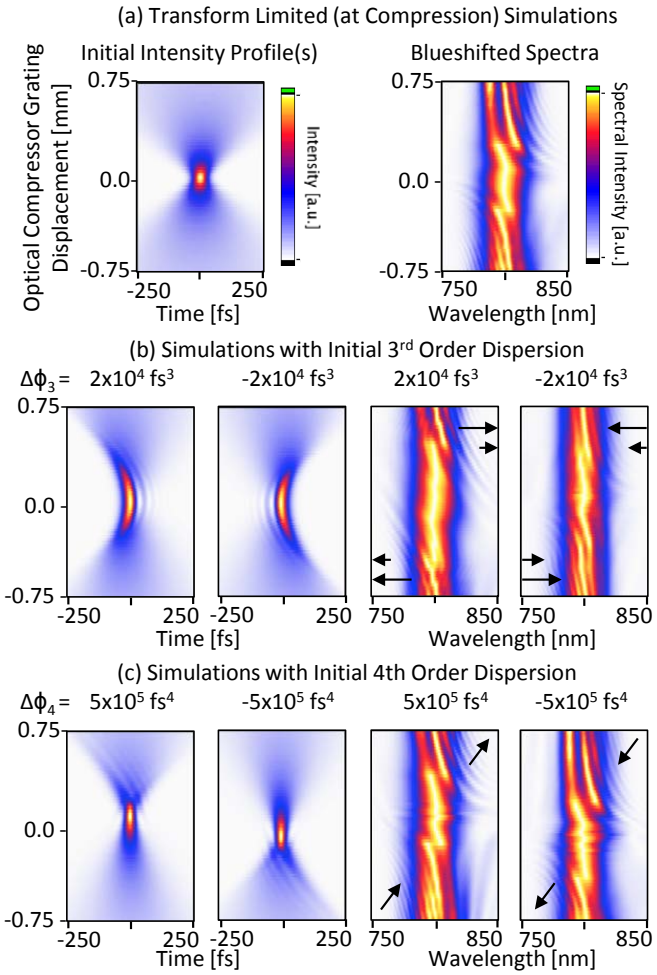

Fig. 4. Five sets of simulations with various initial phases demonstrating the effect of laser system dispersion on pulse shape and on the morphology of blueshifted spectra and the resulting on-axis spectra. All simulated pulses have 80 mJ initial energy. Note that the initial phase added to the pulse is quoted, but phase after compression varies as a function of compressor grating spacing. Arrows are added to the blueshifted spectra to indicate how the morphology with added initial spectral phase differs from that with no dispersion.

reducing the number of fringes in the morphology. This appears as a stretching or contracting of the blueshift pattern versus grating separation. This can be understood in the time domain because added high order phase creates a larger phase difference between the front of the pulse and the rear. Because the pulse is otherwise transform limited, the quoted initial third order phase is also the phase at compression; the same is true for initial fourth order phase.

Initial fourth order phase ϕ_4 creates asymmetry in the intensity profile and nonlinear chirp with respect to peak compression. It adds pre-/post-pulses to the intensity profile on one side of compression and reduces the chirp of the main beam, reducing the resulting spectral interference fringes. On the other side of compression, it adds extended tails to the intensity profile, and the main pulse remains chirped (Fig. 4c intensity profiles), adding spectral interference fringes.

4. BLUESHIFT AS A LASER DIAGNOSTIC

The blueshift morphology is in principle sensitive to pulse energy and density distribution as well as spectral phase, and these must be independently determined to ensure a good fit to the spectral phase. To determine the actual spectral phase of the laser, FROG measurements [6] of the compressed laser pulses were made at a range of optical compressor settings [26]. The spectral phase of the laser was determined from these measurements, which is the input for the following simulations. The match in blueshift morphology between experiment and simulations confirms that the spectral phase at focus is the same at that measured by the FROG, which samples the beam after propagation through a vacuum window and a collimating lens.

Spectral blueshifting was measured at BELLA with a 1.5 cm slit gas jet target with a known density distribution. The expanding gas jet density profile was measured 10 mm from the slit jet (the distance from the laser axis to the jet face) by high pressure neutral gas interferometry and is shown in Fig. 5 scaled to the pressure used in the blueshifting experiments. The uncertainty in the measured profile is estimated to be $\lesssim$10%. Since the slit jet lacks rotational symmetry, the profile was determined by tomographic reconstruction of 166 angular views of the jet plume [28]. The ionizing region in a focusing laser pulse, where blueshifting occurs, will vary as the pulse focuses and its intensity changes. As the chirped pulse focuses, the region of spectrum that is blueshifted will change. The shifted spectrum of a focusing chirped pulse is therefore sensitive to the spatial distribution of neutral gas on the length-scale over which pulse intensity changes, the laser's Rayleigh length Z_R. The ionizing laser beam had an aperture in the near field to enlarge the focal spot to 85 μm and make its focal depth longer than the jet, so the spectra are relatively insensitive to the density profile except for its integrated density. The simulated profile was a constant density plateau of the same full width at half maximum (FWHM) and integrated density as the measured profile. The plateau helium density was $n_{atomic} = 1.3 \times 10^{18}$ cm^{-3} and profile FWHM was 2.05 cm.

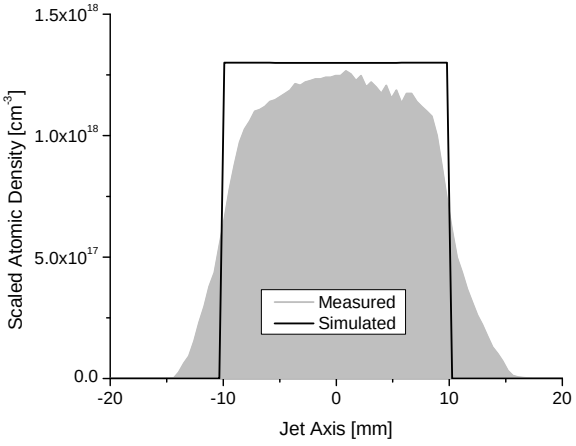

Fig. 5. The measured on-axis density from the 1.5 cm slit jet a distance 10 mm away from the jet outlet is shown in grey scaled to the backing pressure used in the experiment. The simulated density profile, with the same FWHM and integrated density is shown in black.

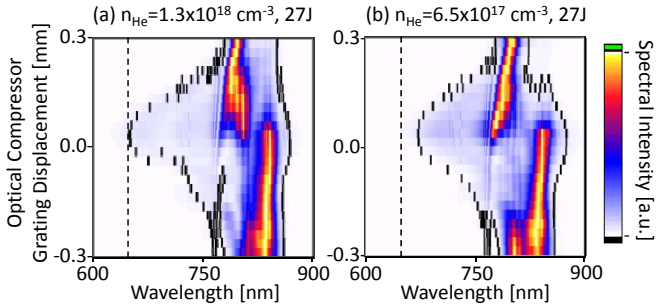

Fig. 6. Simulated blueshifted spectra from 27mJ pulses as a function of compression at (a) the measured density ($n_{He} = 1.3 \times 10^{18}$ cm^{-3}) and (b) 50% lower density ($n_{He} = 6.5 \times 10^{17}$ cm^{-3}). The solid lines indicate the 2% intensity level for each of the individually normalized spectra. The dashed lines indicate the maximum extent of blueshifting for the 1.3×10^{18} cm^{-3} case.

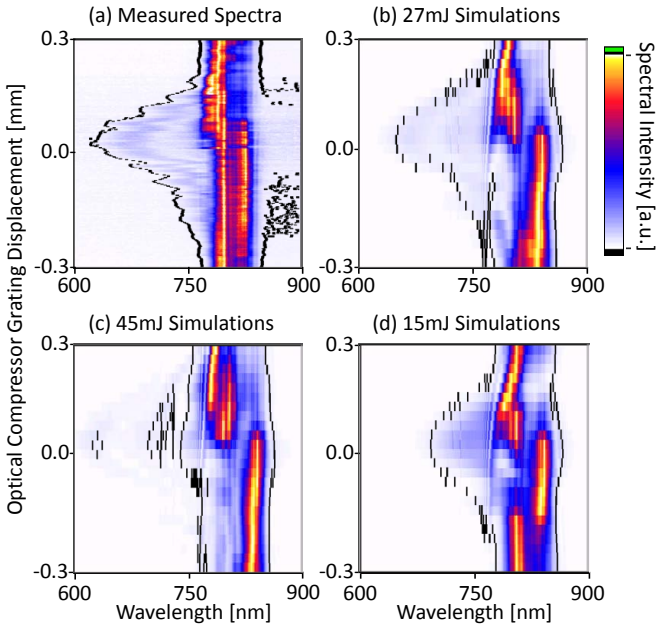

Fig. 7. (a) Measured normalized spectra as a function of optical compressor grating spacing. (b) Simulated 27 mJ pulses, which show the closest match to the measured spectra. (c) Simulated 45 mJ pulses underestimate the fraction of energy in the blueshifted light while (d) simulated 15 mJ pulses underestimate extent of spectral shifting. The solid lines indicate the 2% intensity level for set of spectra.

The effect of density is shown in Fig. 6. In Fig. 6a, the blueshifting resulting from the simulated density profile in Fig. 5 is shown, while in 6b the simulated density is lowered by 50% to $n_{He} = 6.5 \times 10^{17}$ cm^{-3}. Lowering the density results in a noticeable reduction in the maximum spectral shift, consistent with expectations from Eqn. 2. This effect is observed at other energies as well. Because the magnitude of spectral change is moderate, as seen by the small change in the 2% threshold for a large (50%) change in density, it is expected that the much smaller errors on the density measurement are not a significant source of error in matching simulations to measured spectra.

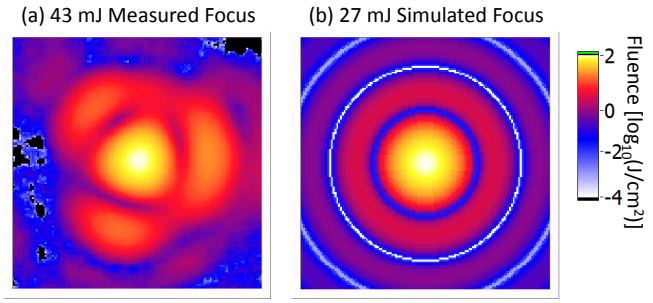

Fig. 8. The (a) measured focal spot with energy 43 mJ and (b) simulated focal spot with energy 27 mJ and the same size. The color scale was chosen to highlight low intensity features.

The dependence on energy is demonstrated in Fig. 7, in which (a) measured spectra (individually normalized to their peak intensity) are compared with (b) simulations of 27 mJ pulses (corresponding to the measured energy). Simulations with (c) more energy show a worse fit to the measured spectra at 45 mJ, based on the 2% intensity profile, and (d) with less energy show an underestimation of the blueshifting at 15mJ. When the energy is wrong, the simulation under/overestimates the wavelength shift in the bulk of the spectrum, which leads to a worse fit with the data. The solid lines indicate the smoothed contour at 2% of peak intensity of the spectrum.

The measured energy of the apertured laser, accounting for transmission losses, was determined to be 43 mJ at target. The profile of the pulse used in the experiment, shown in Fig. 8a, was significantly different from the Airy pattern modeled in the simulations and contained considerably more energy in the wings of the pulse. A simulated pulse with an Airy pattern radial distribution, shown in Fig. 8b and corresponding to a flat top near field distribution with flat phase, was determined to match the on-axis fluence of the 43 mJ measured pulse when the simulated energy was 27 mJ. For this reason, 27mJ will be used as the pulse energy for the subsequent simulations.

Known dispersion was added to the ionizing laser to investigate limits on the sensitivity of this technique to different orders of phase. The total phase of the laser including the added dispersion is known, because the laser's initial phase (without added dispersion) was determined by multiple FROG measurements at various grating spacings and the dispersions add linearly to this. Spectral dispersion was introduced with a Fastlite DAZZLER acousto-optical modulator [29]. The optical compressor grating spacing was varied, in addition to the fixed dispersion from the DAZZLER, and the resulting blueshifted spectra of ionizing pulses were measured to determine their morphology. The optical compressor varied pulse length from a (measured) minimum of 34 fs to a (calculated) maximum of 120 fs in the absence of added dispersion. A scan of grating spacing is shown in Fig. 9a, and the matching simulations of 27 mJ pulses with the same initial phase is shown in Fig. 9b. Their agreement for this and other introduced dispersions (see Figs. 10 and 11) indicates the validity of the model in this regime.

To quantify the morphology's sensitivity to phase it is necessary to establish a metric for quality of fit. The relevant qualitative features of the shifted spectra vary with the specifics of the experiment. For blueshifting in the gas jet, the relevant features of the morphology are the range of compression that gives blueshifting and the shape of the spectrum. Based on these fea-

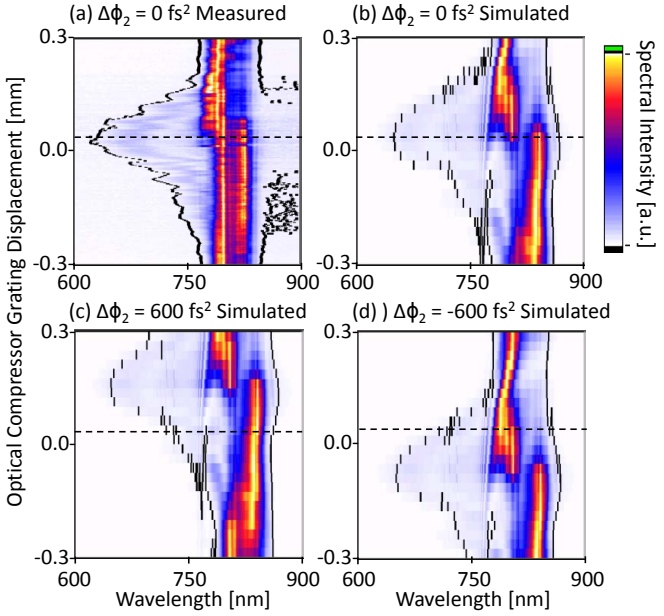

Fig. 9. Normalized blueshifted spectra from a pulse with varying optical compression without added dispersion (a) measured at BELLA and (b) simulated with the same measured spectral phase. Mismatched simulations with (c) +600 fs^2 or (d) -600 fs^2 of added second order dispersion to demonstrate the sensitivity of the technique. The solid lines indicate the 2% intensity level for each spectrum, and the dashed line indicates the position with the maximum blueshift in the measured spectra.

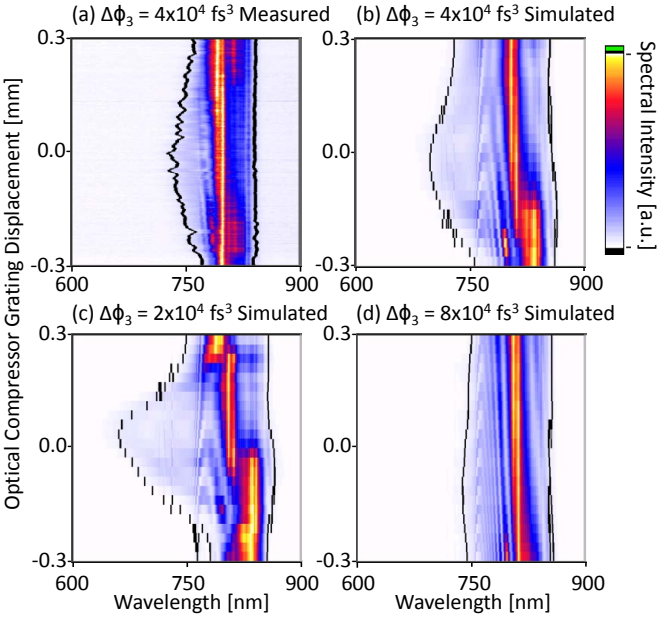

Fig. 10. Normalized blueshifted spectra from a pulse with added third order spectral dispersion (a) measured at BELLA and (b) a simulation with same added initial spectral phase $\Delta\phi_3 = 4 \times 10^6$ fs^3. Mismatched simulations with (c) less dispersion $\Delta\phi_3 = 2 \times 10^6$ fs^3 and (d) more dispersion $\Delta\phi_3 = 8 \times 10^6$ fs^3 show the changes in spectral morphology with third order dispersion. The solid lines indicate the 2% intensity level for each spectrum.

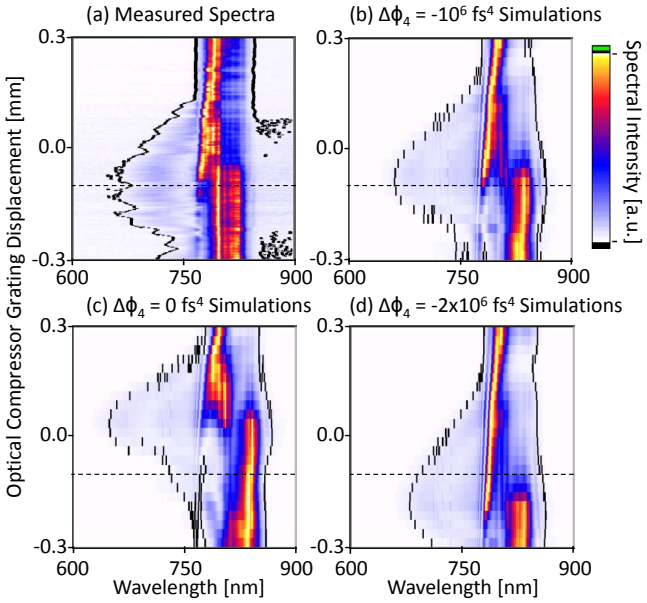

Fig. 11. Normalized blueshifted spectra from a pulse with added fourth order spectral dispersion (a) measured at BELLA and (b) a simulation with same added initial spectral phase $\Delta\phi_4 = 10^6\,\mathrm{fs}^4$. Mismatched simulations to demonstrate sensitivity with (c) less dispersion $\Delta\phi_4 = 0\,\mathrm{fs}^4$ and (d) more dispersion $\Delta\phi_4 = 2\times10^6\,\mathrm{fs}^4$ differ in the morphology of the blueshifted spectra. The solid lines indicate the 2% intensity level for each spectrum, and the dashed line indicates the position with the maximum blueshift in the measured spectra.

tures, sensitivity to dispersion can be established for each order by determining the minimum change required for a subjective change in the morphology. As an example of the technique's sensitivity to second order phase, mismatched simulations are shown in Figs. 9c and 9d. The blueshifted spectral pattern shifts up or down, respectively, relative to the compressed location for pulses without added dispersion, but the spectral morphology stays unchanged apart from the shift. In contrast, the spectral morphology changes dramatically with third order dispersion, as shown in 10a and its matching simulation 10b. Adding less third order phase as in Fig. 10c or more third order phase as in Fig. 10d causes large changes in the spectral morphology, which establish bounds on the sensitivity of the technique to third order phase. The addition of fourth order phase significantly changes both the spectral morphology and the grating location that gives the largest blueshift. The measurements in Fig. 11a and the matching simulation in Fig. 11b show that blueshifting occurs at a different location and over a wider range of compressor grating spacings compared with Figs. 11c/9b, which has no added dispersion. The disagreement of simulations 11c and 11d with the data, in comparison with the agreement between Figs. 11a and 11b, shows how well the fourth order sensitivity can be determined. Conservative limits for sensitivity to each order of spectral phase based on fits to the gas jet blueshifted spectra are summarized in Table 1.

5. CONCLUSION

An iterative algorithm to guess a spectral phase, simulate it for several values of compression, and compare the results with experiment would allow direct determination of the initial phase from the blueshifted measurements, but its application is constrained by the computational resources required for simulating the laser's self-consistent propagation. In the absence of such a method to determine the best fit to a given set of blueshifted spectral measurements, the sensitivity of blueshifting morphology is limited to changes in spectral phase that produce gross effects in the blueshifted morphology (see Figs. 7-9). The ability to set conservative limits such as those noted in Table 1 is still sufficient to crosscheck the spectral phase at laser focus/target measured by a second diagnostic at another location, such as FROG or SPIDER, or to provide a day-to-day consistency check of spectral phase.

Table 1. Blueshifting sensitivity to spectral dispersion based on simulated scans of grating spacing

Phase Order	Uncertainty
2^{nd}	$\pm 600 fs^2$
3^{rd}	$\pm 4\times10^4 fs^3$
4^{th}	$\pm 10^6 fs^4$

In summary, a new technique is proposed for verifying the high-order spectral phase of a laser system based on the morphology of ionization blueshifting in a known gas target as a function of compression. The blueshifted spectra for different pulse compressions are straightforward to measure, and this technique allows characterization of the spectrum in-situ at the high-power laser's focus, making it particularly suited for laser plasma acceleration studies. The orders of the laser's spectral phase have distinct effects on the spectral morphology and can be tested via numerical simulation of the process given a known target density. This is demonstrated by agreement between simulations and data from the Berkeley Lab Laser Accelerator (BELLA).

Funding.

This work was supported by the Director, Office of Science, Office of High Energy Physics, of the U.S. Department of Energy under Contract No. DE-AC02-05CH11231 and the National Science Foundation under Award No. PHY-1415596.

Acknowledgement.

The authors would like to thank Nicholas H. Matlis for several helpful discussions and foundational understanding.

REFERENCES

1. E. Esarey, C. B. Schroeder, and W. P. Leemans, "Physics of laser-driven plasma-based electron accelerators," Rev. Mod. Phys. 81, 1229-1285 (2009)
2. P. Gibbon, "High-Order Harmonic Generation in Plasmas," IEEE QE 33, 1915-1924 (1997)
3. D. Strickland and G. Mourou, "Compression of amplified chirped optical pulses," Opt. Comm. 56, 219-221 (1985)
4. W. P. Leemans et al., "Electron-Yield Enhancement in a Laser-Wakefield Accelerator Driven by Asymmetric Laser Pulses," Phys. Rev. Lett. 89, 174802 (2002)
5. I. A. Walmsley and C. Dorrer, "Characterization of ultrashort electromagnetic pulses," Adv. Opt. Photonics 1, 308-437 (2009)
6. R. Trebino et al., "Measuring ultrashort laser pulses in the time-frequency domain using frequency-resolved optical gating," Rev. Sci. Instrum. 68, 3277-3295 (1997)

7. C. Iaconis and I.A. Walmsley, "Spectral phase interferometry for direct electric-field reconstruction of ultrashort optical pulses," Opt. Lett. 23, 792-794 (1998)
8. E. T. J. Nibbering et al., "Spectral determination of the amplitude and the phase of intense ultrashort optical pulses," JOSA B 13, 317-329 (1996)
9. S.P. LeBlanc and R. Sauerbrey, "Spectra, temporal, and spatial characteristics of plasma-induced spectral blue shifting and its application to femtosecond pulse measurement," JOSA B 13, 72-88 (1996)
10. S.P. LeBlanc and R. Sauerbrey, "Spectral blue shifting of a femtosecond laser pulse propagating through a high-pressure gas," JOSA B 10, 1801-1809 (1993)
11. S. C. Wilks et al., "Photon Accelerator," Phys. Rev. Lett. 62, 2600 (1989)
12. C. D. Murphy et al., "Evidence of photon acceleration by laser wake fields," Phys. of Plas. 13, 033108 (2006)
13. S.P. LeBlanc et al., "Spectral blue shifting of a femtosecond laser pulse propagating through a high-pressure gas," JOSA B 10, 1801-1809 (1993)
14. P. Chessa et al., "Temporal and Angular Resolution of the Ionization-Induced Refraction of a Short Laser Pulse in Helium Gas," Phys. Rev. Lett. 82, 552 (1999)
15. E. Esarey, G. Joyce, and P. Sprangle, "Frequency up-shifting of laser pulses by copropagating ionization fronts," Phys. Rev. A 44, 3908-3911 (1991)
16. X. M. Tong and C. D. Lin, "Empirical formula for static field ionization rates of atoms and molecules by lasers in the barrier-suppression regime," J. Phys. B: At. Mol Opt. Phys. 38, 2593-2600 (2005)
17. M.V. Ammosov, N.B. Delone, and V.P. Krainov, "Tunnel ionization of complex atoms and of atomic ions in an alternating electromagnetic field," Sov. Phys. JETP 64, 1191-1194 (1986)
18. C. Benedetti et al., "Efficient Modeling of Laser-Plasma Accelerators with INF&RNO," in Proc. of the 14th Advanced Accelerator Concepts Workshop, Annapolis, MD, USA, June 13-19, 2010, AIP Conf. Proc. 1299, 250 (2010)
19. C. Benedetti et al., "Efficient modeling of laser-plasma accelerators using the ponderomotive-based code INF&RNO," in Proceedings of ICAP2012, Rostock-Warnemünde, Germany (JACoW, Geneva, 2012) p. THAAI2
20. S. Steinke et al., "Staging of laser-plasma accelerators," Phys. Plasmas 23, 056705 (2016)
21. S. Steinke et al., "Multistage coupling of independent laser-plasma accelerators," Nature 520, 190-193 (2016)
22. A.J. Gonsalves et al., "Tunable laser plasma accelerator based on longitudinal density tailoring," Nature Physics 7, 862-866 (2011)
23. S. Shiraishi et al., "Laser red shifting based on characterization of wakefield excitation in a laser-plasma accelerator," Phys. Plasmas 20, 063103 (2013)
24. W.P. Leemans et al., "Multi-GeV Electron Beams from Capillary-Discharge-Guided Subpetawatt Laser Pulses in the Self-Trapping Regime," Phys. Rev. Lett. 113, 245002 (2014)
25. C. Fiorini et al., "Temporal Aberrations Due to Misalignments of a Stretcher-Compressor System and Compensation," IEEE J. QE 30, 1662-1670 (1994)
26. K. Nakamura et al., in AIP Conference Proceedings, 16th Advanced Accelerator Concepts Workshop, San Jose, 2014 (AIP, in press)
27. J. K. Wahlstrand, Y. H. Chen, and H. M. Milchberg, "High Field Optical Nonlinearity and the Kramers-Kronig Relations," Phys Rev. Lett. 109, 113904 (2012)
28. P. C. Hansen and M. Saxild-Hansen, "AIR Tools - A MATLAB Package of Algebraic Iterative Reconstruction Methods," J. Comput. App. Math. 236, 2167-2178 (2012)
29. F. Verluise et al., "Amplitude and phase control of ultrashort pulses by use of an acousto-optic programmable dispersive filter: pulse compression and shaping," Opt. Lett. 25, 575-577 (2000)
30. J.R. Feinup, "Phase retrieval algorithms: a comparison," Appl. Opt. 21, 2759-2769 (1982)